CrossMark

Effect of Overaging on Fatigue Crack Propagation and Stress Corrosion Cracking Behaviors of an Al-Zn-Mg-Cu Alloy Thick Plate

Lianghua Lin, Zhiyi Liu, Xiangnan Han, and Wenjuan Liu

The fatigue property as well as stress corrosion cracking (SCC) resistance of an Al-Zn-Mg-Cu alloy thick plate in peak-aged and overaged tempers (T7351 and T7651) is systematically investigated by fatigue crack propagation (FCP) test and slow strain rate test (SSRT). Microstructural characterization is examined by transmission electron microscopy and scanning electron microscopy. Results reveal that the T7351 alloy has lower strength but higher electrical conductivity as compared to T7651 alloy. The FCP resistance of T7351 alloy is superior to that of the T7651 alloy due to the coarser precipitates in the highly overaged alloy in which the strain localization is reduced by promoting homogeneous slip. In addition, the SSRT test suggests a higher SCC resistance in T7351 alloy. The enhanced SCC resistance is found to depend on grain boundary precipitate characteristics and crack propagation resistance of the alloys.

1. Introduction

Al-Zn-Mg-Cu alloys are widely used for aerospace applications due to their high strength-to-weight ratio and excellent fracture toughness. The strengthening of these heat-treatable alloys is predominately determined by the type and dimension of precipitates formed during aging (Ref 1). The precipitation sequence in Al-Zn-Mg-Cu alloys can be summarized as (Ref 2, 3): super-saturated solid solution → Guinier–Preston (G.P.) zones → metastable η' phase → equilibrium η phase. All these phases have been extensively investigated and their features are well assessed in previous studies (Ref 4-6). In general, the G.P. zones contribute to part of hardening as well as acting as the precursors for η' precipitates. The intermediate η' precipitates are thought to play a major role on strengthening due to its fine dispersion within grains. With further aging, η' phase will transform to equilibrium η phase. In addition, the stable η precipitates can form directly on dispersions and grain boundaries during slow quenching. These coarse η precipitates lead to a reduction in strength and have substantially influenced on corrosion susceptibility (Ref 7, 8).

Although high-strength Al-Zn-Mg-Cu alloys possess good resistance to uniform corrosion, they are prone to stress corrosion cracking (SCC) in chloride-containing environment. Extensive investigations on the SCC behavior of aluminum alloys show that the SCC resistance is determined by the morphology and chemistry of grain boundary precipitates (Ref 8, 9), the distribution of dislocations (Ref 10) and the segregation of alloying elements along grain boundaries (Ref 11, 12). Several heat treatments such as multi-step overaging (Ref 13, 14), retrogression and re-aging (RRA) (Ref 10) and secondary aging (Ref 9) have been developed to achieve good SCC resistance. However, they still fail to obtain the desirable performance. For instance, overaging reduces strength by 10-15% (Ref 14), and RRA treatment is technically difficult for large components due to the transitory high-temperature processes (Ref 10).

For a long time, two-step aging treatments are used to improve SCC resistance of commercial Al-Zn-Mg-Cu alloys. In these tempers, aging treatment at one low temperature is followed by second aging at higher temperature. In first-stage aging, the temperature is always below the solvus of G.P. zones to ensure its uniform dispersion. In the second stage, the coarse precipitates both within grains and at grain boundaries are obtained. Two well-known examples are T73 and T76 tempers (corresponding tempers are T7351 and T7651 for pre-stretched thick plates) (Ref 15). Although the property discrepancy between overaged and peak-aged Al-Zn-Mg-Cu alloys has been widely investigated, little attention focuses on the influence of different overaging treatments on microstructures and properties. In this paper, therefore, the differences in SCC and FCP behavior between the T7351 and T7651 alloys are well explored. Comparison with the peak-aged alloy is also provided to explain the intrinsic mechanism.

2. Experimental Procedures

The material used in the present work is a commercial 7475 alloy plate with a thickness of 18 mm. The chemical composition is 6.1 wt.% Zn, 2.5 wt.% Mg, 1.8 wt.% Cu, 0.25 wt.% Cr, 0.04 wt.% Ti and balance Al. The plates were solution treated at 470 °C for 1 h, cold water quenched and then aged to T651, T7651 and T7351 tempers as described in Table 1. The

Lianghua Lin, School of Material Science and Engineering, Central South University, Changsha 410083, People's Republic of China; and School of Mechanical and Electronic Engineering, East China University of Technology, Nanchang 330013 Jiangxi, China; **Zhiyi Liu, Xiangnan Han**, and **Wenjuan Liu**, School of Material Science and Engineering, Central South University, Changsha 410083, People's Republic of China. Contact e-mail: liuzhiyi@csu.edu.cn.

Table 1   Summary of heat treatments

Tempers	The processing of heat treatments
T651	470°C × 1 h + quenching + 2% pre-stretching + 120 °C × 24 h
T7651	470°C × 1 h + quenching + 2% pre-stretching + 125 °C × 3 h + 170 °C × 10 h
T7351	470°C × 1 h + quenching + 2% pre-stretching + 120 °C × 8 h + 160 °C × 30 h

overaging parameters were chosen according to the standard ASM 2772 and Ref 13. Specimens for tensile test were prepared vertical to the rolling direction of the plate with a gauge length of 30 mm. Tensile properties were measured on a CMT5105 electronic universal testing machine at ambient temperature with 2 mm/min loading speed, and three specimens were tested to obtain an average value. For electrical conductivity measurements, specimens of dimensions of 20 mm × 20 mm were cut from the plate. These specimens were ground progressively using 220, 600, 1000 and 1500 grit SiC grinding papers, followed by degreased with ethanol and dried prior to testing. The electrical conductivity test was determined by D60K digital conductivity meter, reported as a percentage of the International Annealed Copper Standard (%IACS). At least three specimens of each heat-treated temper were tested to obtain an average value.

To obtain the FCP rate (da/dN), the preparation of specimens follows the ASTM E-647 standard. All specimens were performed using compact tension (C-T) specimens taken from the plates in the L–T orientation. Fatigue crack growth test was carried out at a stress ratio ($R = K_{min}/K_{max}$) of 0.1 with a loading frequency of 10 Hz on a MTS-810 test machine. The slow strain rate test (SSRT) was performed to determine the SCC resistance of the studied alloy subjected to various heat treatments. The tests were carried out at the strain rates of 5.0×10^{-6} s^{-1} in air and in 3.5% NaCl aqueous solution, respectively.

The specimen fracture surface was observed by FEI Quanta 200 scanning electron microscopy (SEM) with an operating voltage of 20 kV. The specimens were also investigated by a TecnaiG^{2}20 transmission electron microscope (TEM) operating at 200 kV. Thin foils for TEM characterization were prepared by double-jet electropolishing at 20 V in a solution of 30% nitric acid and 70% methanol solution at about − 25 °C.

3. Results and Discussion

3.1 Microstructures

Figure 1 shows the representative bright-field TEM micrographs and corresponding selected area electron diffraction (SAED) patterns of precipitates in various heat-treated Al-Zn-Mg-Cu alloys. All the TEM images are obtained along the $[100]_{Al}$ zone axis. In peak aging condition (T651), fine and dense precipitates are observed in grain interior. These small spherical precipitates can be identified as G.P. zones and η' phase as weak diffraction spots at 1/3(2/3) $\{220\}_{Al}$ and $\{1, (2n + 1)/4, 0\}_{Al}$ positions could be observed from corresponding SAED patterns. In Fig. 1(b), the TEM micrograph of T7651 alloy contains a number of spherical precipitates within the

grains. Clear diffraction spots at 1/3(2/3) $\{220\}_{Al}$ positions indicate that η' precipitates dominate the microstructure. For T7351 alloy, the SAED patterns suggest that η' phase is still predominant. Compared to T7651 alloy, however, η' precipitates in T7351 alloy become larger and its number density decreases, as shown in Fig. 1(c).

The typical morphologies of precipitates at the grain boundaries of Al-Zn-Mg-Cu alloy after different treatments are presented in Fig. 1(d-f). The grain boundary precipitates in T651 alloy are continuously distributed and no clear precipitation free zone (PFZ) is found in Fig. 1(d). Inversely, the grain boundaries of both T7651 and T7351 alloys are decorated with coarse and discontinuously η phase. The two overaged alloys also exhibit PFZs at grain boundaries with 80-120 nm in size (see Fig. 1e, f). A careful examination reveals that the wide of PFZ in T7351 alloy is slightly larger than that in T7651 one. This discrepancy in PFZ may be ascribed to the longer aging time in T7351 alloy.

3.2 Tensile Properties and Electrical Conductivity

The tensile properties and electrical conductivity of Al-Zn-Mg-Cu alloys in various conditions are shown in Table 2 and Fig. 2. It can be seen that the T651 alloy has the highest ultimate tensile strength of 561 MPa. Compared with T651 alloy, reduced tensile strength and elongation in both overaged alloys are found. In particular, the strength value decreases by 6 and 9% for T7651 and T7351 tempers, respectively. These results are in consistent with other work in the Al-Zn-Mg-Cu system alloys (Ref 16) and agree well with the microstructures observed in Fig. 1. For example, the highest strength of T651 alloy is attributed to the high density of coherent G.P. zones and semi-coherent η' precipitates according to the shearing mechanism (Ref 6, 17). When the alloy is subjected to overaging, the unstable G.P. zones disappear, accompanied by the transformation from stable G.P. zones to η' phase. Subsequently, the formation and coarsening of equilibrium η phase are observed. Coarse precipitates are less effective in hindering the dislocation movement and reducing the alloy strength. Thus, T7351 alloy has relatively lower strength as compared to T7651 alloy.

The electrical conductivity values of Al-Zn-Mg-Cu alloy in various conditions are presented in Fig. 2. The electrical conductivity values of T651, T7651 and T7351 alloys are 36% IACS, 40.5% IACS and 42% IACS, respectively. It is found that the alloy with high electrical conductivity has low tensile strength. Measuring electrical conductivity is an effective method to investigate the microstructure of aged alloys (Ref 18). In general, electrical conductivity values are directly related to many microstructural factors such as dislocation density, vacancy concentration, precipitate size and volume fraction with different aging treatments (Ref 13, 18). These factors cause the localized strain fields in the crystalline lattice, thus affecting the intensity of electron scattering. In any cases, an increase in electron scattering will lead to a decrease in electrical conductivity. In present work, the T651 alloy exhibits high density of coherent G.P. zones and semi-coherent η' precipitates which results in the lowest electrical conductivity, as seen in Fig. 1 and 2. After overaging, G.P. zones transform to η' phase and the coarse precipitates form. These larger precipitates within grains imply the lower intensity of electron scattering. Hence, overaging leads to an increase in electrical conductivity.
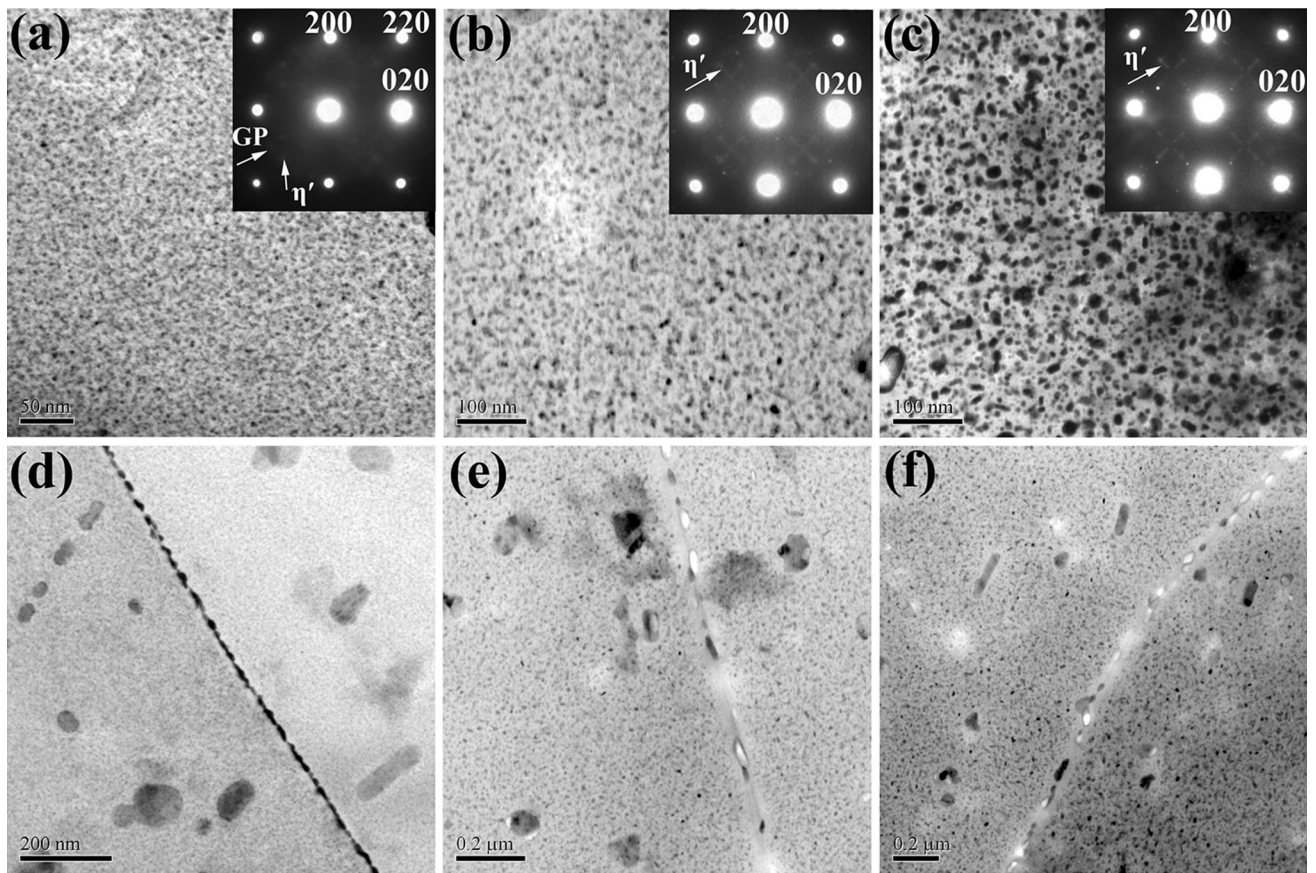
Fig. 1 Representative TEM micrographs showing the matrix and grain boundaries precipitates of Al-Zn-Mg-Cu alloys in (a, d) T651, (b, e) T7651 and (c, f) T7351 conditions, viewed along the $<100>_{Al}$ zone axis

Table 2 Tensile properties and electrical conductivity of the studied Al-Zn-Mg-Cu alloy

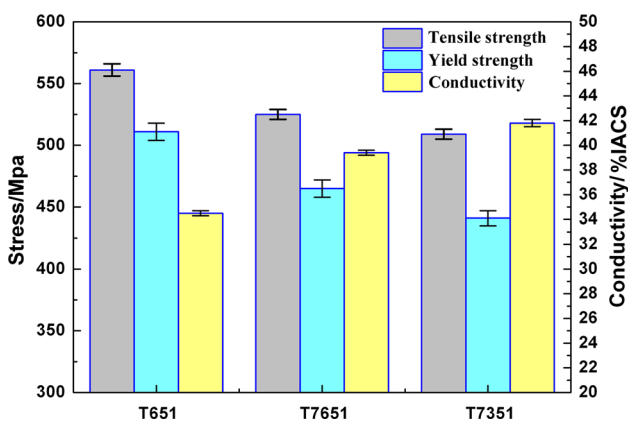| Tempers	Tensile strength, MPa	Yield strength, MPa	Elongation, %	Electrical conductivity, %IACS
T651	561 ± 4	511 ± 6	15.5 ± 0.2	34.5 ± 0.2
T7651	525 ± 3	465 ± 6	13.5 ± 0.2	39.4 ± 0.2
T7351	509 ± 3	441 ± 5	14.9 ± 0.2	41.8 ± 0.3

Fig. 2 Effects of different aging treatments on the tensile properties and electrical conductivity of Al-Zn-Mg-Cu alloy

Further, larger precipitates in T7351 alloys are responsible for its higher electrical conductivity as compared to T7651 alloy.

3.3 Fatigue Crack Propagation Behavior

Figure 3 illustrates the FCP rates for two overaged Al-Zn-Mg-Cu alloys. The curves for both alloys reveal the same trend that the FCP rate increases as ΔK increases. The FCP behavior can be described in three typical regions with respect to the crack growth characteristic: (1) threshold region where the FCP rate is quite low; (2) Paris regime where FCP rate is approximately linear with ΔK and (3) the accelerated FCP region. As shown in Fig. 3, a higher threshold value with a relatively lower FCP rate is obtained by T7351 temper rather than T7651 alloy. For example, the FCP rate of T7651 alloy is approximately 1.14×10^{-4} mm/cycle, much higher than T7351 alloy (0.75×10^{-4} mm/cycle) at $\Delta K = 15$ MPa m$^{0.5}$. Pronounced differences in FCP rates between two overaged alloys remain throughout the applied stress intensity, indicating the FCP resistance of T7351 alloy is superior to that of T7651 alloy.

Figure 4 shows the typical fatigue fracture surfaces of T7361 and T7351 alloys at different ΔK levels. In near-threshold regime, both crack surfaces display similar morphol-

ogy containing flat facets areas where numerous tear ridges are observed. These shear ridges are parallel to the fatigue crack growth direction, joined by many micro-voids. As seen in Fig. 4(a) and (d), large fatigue plateaus are evident in T7351 alloy with respect to T7651 alloy. Normally, the crack facet appearance is associated with the accumulated plastic strain between the matrix and the particle interface during loading (Ref 19). The formation of voids is presumably due to the localized plastic deformation through the interaction of dislo-
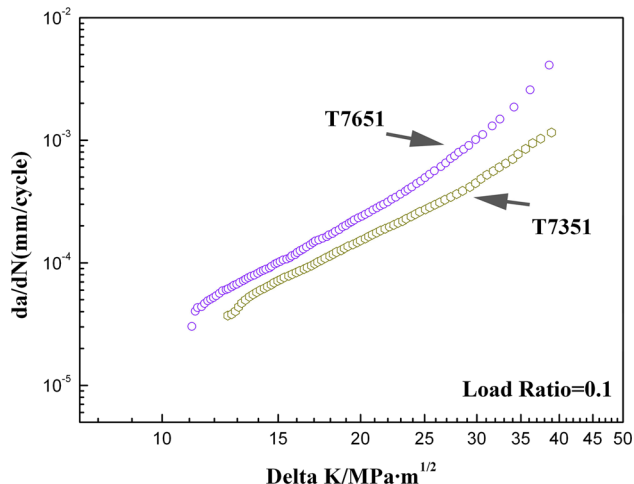

Fig. 3 Fatigue crack propagation rates (da/dN) vs. applied stress intensity factor range (ΔK) curves of Al-Zn-Mg-Cu alloys in T7651 and T7351 tempers

cations and coarse particles. In Fig. 4(b) and (e), well-defined striations, characteristic of Paris regime, are clearly observed in both samples. At a constant value of $\Delta K = 23$ MPa m$^{0.5}$, the average striations spacing are 0.56 and 0.39 μm for T7651 and T7351 alloys, respectively. Obviously, the striation distance in T7351 alloy is shorter than T7651 alloy. Since the average rate of crack propagation is predicted to be inversely proportional to the fatigue striation spacing (Ref 20), the narrow striation spacing in Fig. 4(e) reveals the low FCP rate in T7351 alloy. This result is in consistent with Fig. 3. Furthermore, at this fatigue stage, many secondary cracks are found around coarse second particles in fatigue propagation region. Previous work by Bai et al. (Ref 21) suggested that secondary cracks can reduce the crack driving force and therefore enhance the FCP resistance. However, no obvious difference in the quantity of secondary cracks was observed between the two alloys. Figure 4(c) and (f) shows the typical final fracture appearances of various samples. The fatigue fracture surfaces of both overaged alloys exhibit a dominant ductile fracture mode characterized by dimples. Compared with T7651 alloy, T7351 alloy shows more uniformly distributed dimples and hence better plasticity.

Although many microstructural factors such as alloy texture (Ref 22, 23), grain size (Ref 24), second phases (Ref 25) and precipitates (Ref 26) are reported to affect the FCP behavior, only the precipitate difference is detected between T7651 and T7351 alloys in present work. Therefore, the improved fatigue property for T7351 alloys is apparently related to the precipitates formed during aging process. Extensive investigations have shown that microstructural change induced by aging is a key factor in determining the homogeneity of deformation and
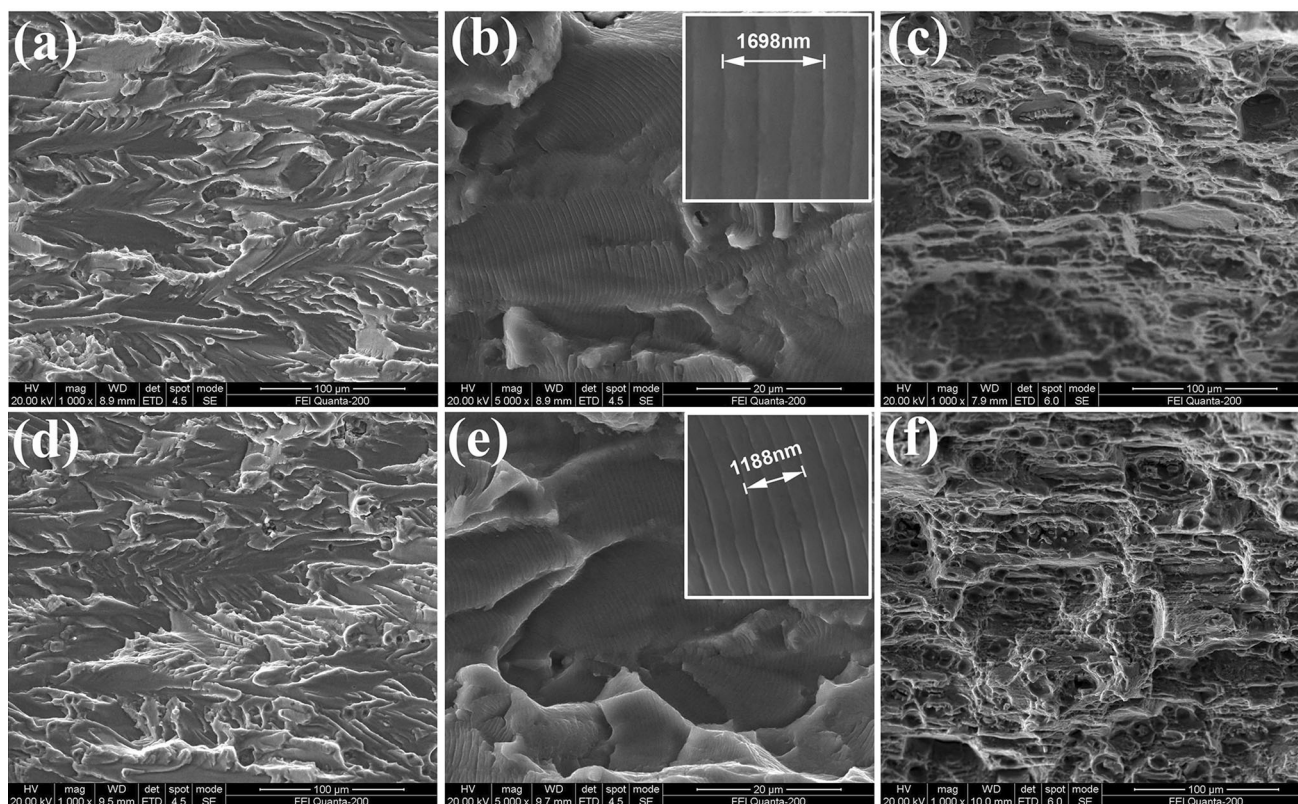

Fig. 4 SEM fractographs of fatigue fracture surface for (a-c) T7651 and (d-f) T7351 alloys. (a, d) in near-threshold regime, (b, e) in Paris regime at ΔK of 23 Mpa m$^{0.5}$ and (c, f) in final fatigue fracture surface. The crack propagation directions are all from left to right
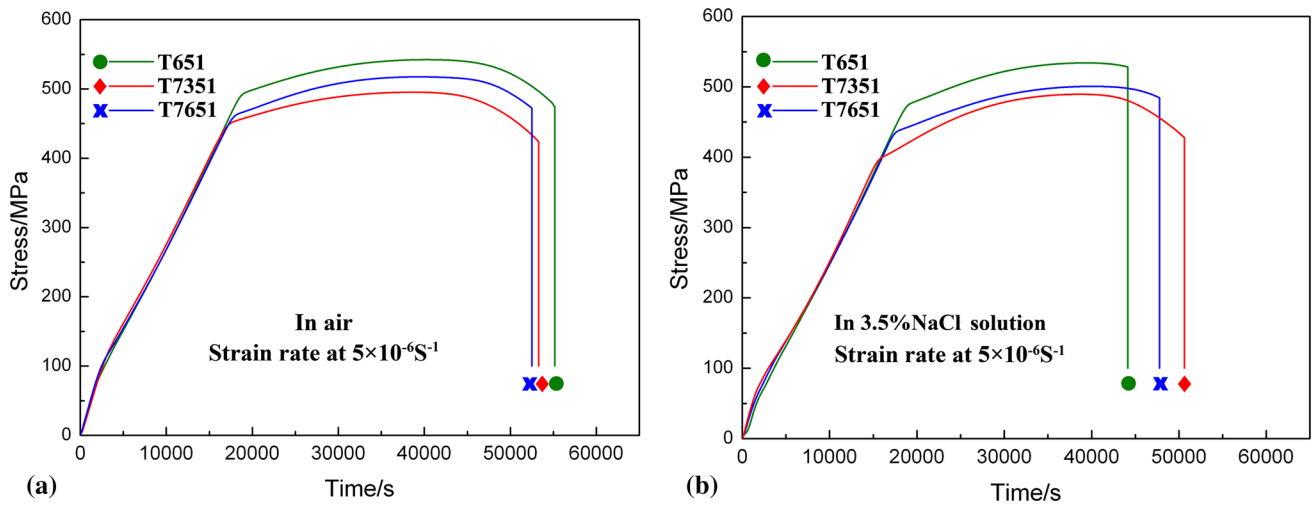
Fig. 5 Typical strain–stress curves of Al-Zn-Mg-Cu alloys in different tempers (a) in air and (b) in 3.5% NaCl solution

Table 3 Results of SSRT for various tempered alloys

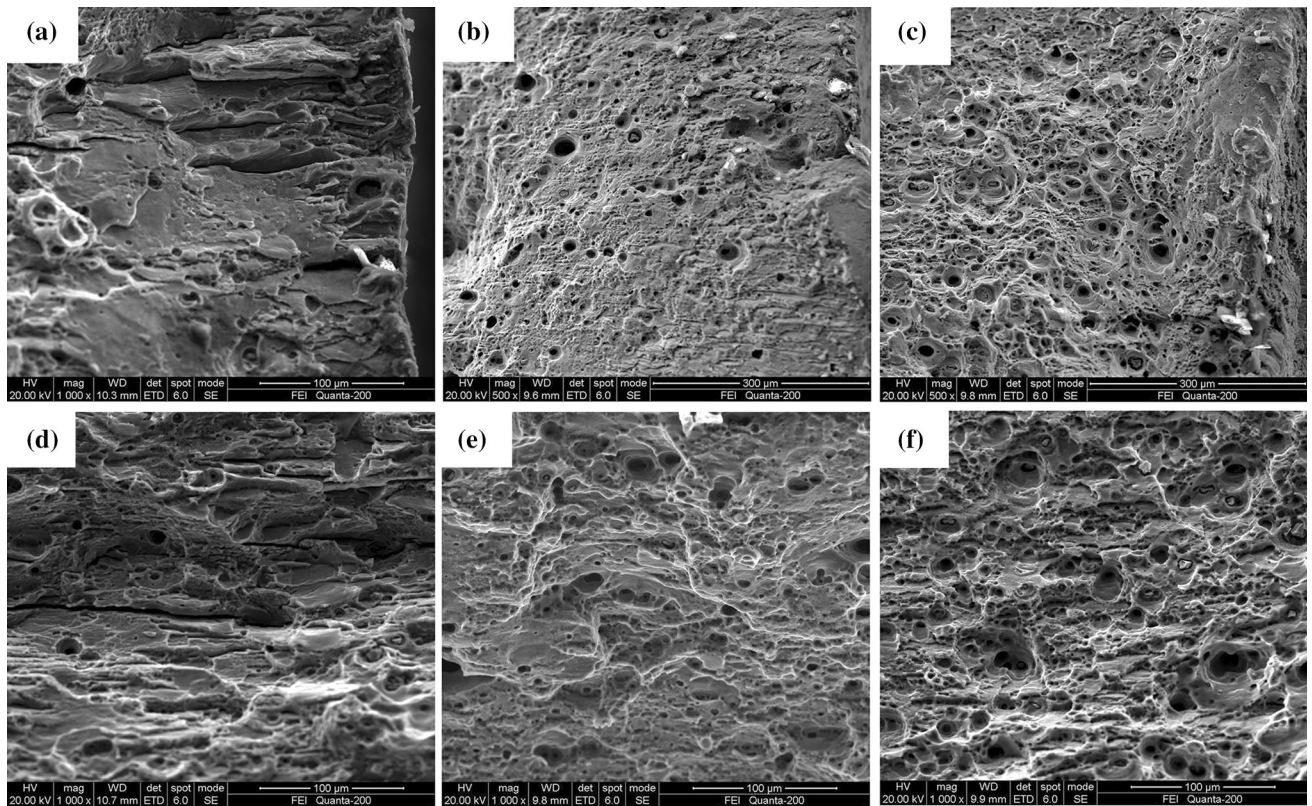| Tempers	Strength, MPa		Time-to-failure (Tf), s		r_{SCC}
	In air	In 3.5% NaCl solution	In air	In 3.5% NaCl solution	
T651	542	534	55,174	44,140	0.80
T7651	517	501	52,510	47,788	0.91
T7351	495	489	53,290	50,632	0.95

Fig. 6 SEM micrographs of SCC fracture of the (a, d) T651, (b, e) T7651 and (c, f) T7351 samples after SSRT tests in 3.5% NaCl solution. (a-c) the edge and (d-f) center of the fracture surface

therefore affect the FCP rates in Al-Zn-Mg-Cu alloys (Ref 27). In general, homogeneous planar slip improves FCP resistance as inhomogeneous planar slip causes strain localization. Particularly, the aging condition is directly related to the precipitate characteristic including the coherency of precipitates with matrix. In underaged condition, the majority of the precipitates are coherent G.P. zones. These coherent precipitates are sheared by dislocations, resulting in strain localization as a consequence of crack nucleation by formation of the shear bands. On the other hand, the main precipitates in the overaged alloys are incoherent η phase and partially coherent η' phase. These non-shearable particles are believed to result in dislocations bypassing. In this case, the cross-slip of dislocations is dominant and the strain localization is relieved. As a result, the deformation becomes more homogeneous and delays the initiation of fatigue crack. Figure 1 shows that much larger η' precipitates are found in T7351 alloy as compared to T7651 alloy. The presence of coarser precipitates reduces the strain localization by promoting homogeneous slip and delays the crack nucleation, finally contributing to the higher FCP resistance for highly overaged alloy. This explanation is further confirmed by the fractographs of fatigue fracture surface in Fig. 4, in which T7351 alloy exhibits more large fatigue plateaus and uniform dimples.

Another factor affecting FCP rate is the width of PFZ near grain boundaries. Since the PFZs are softer than the grains interior (Ref 28), they induce the localized stress concentration during cyclic loading. Hence, PFZs are believed to be sites at which crack initiation takes place preferentially. Therefore, alloys with wide PFZs are more prone to facture in intergranular mode and possess a high FCP rate. In present work, however, the widths of PFZs in two overaged alloys are comparable (Fig. 1). In Fig. 4, it is observed that most of the plateaus are characterize by fatigue striations and the cracks mostly propagate in a transgranular mode. This observation indicates that the PFZ width may have insignificant effect on the FCP rate, especially in high ΔK region. Therefore, the decrease in FCP rate by highly overaging mainly depends on the precipitates within grains.

3.4 Stress Corrosion Crack Resistance

Figure 5 presents the results of slow strain rate test (SSRT) of Al-Zn-Mg-Cu alloys of various tempers in air and 3.5% NaCl solution. When carried out at a strain rates of $5.0 \times 10^{-6} \text{ s}^{-1}$ in air, the typical stress–strain curves for different tempered alloys show a similar trend with that of normal tensile test. In 3.5% NaCl solution, the time-to-failure as well as the ultimate strength decreases as compared to the corresponding samples in air at all conditions. The drop in time-to-failure is due to stress corrosion in aqueous solution, and therefore the ratio of time-to-failure can be used to evaluate the resistance of SCC (r_{SCC}). According to ASTM G129, the r_{SCC} is calculated by following equation:

$$r_{SCC} = \frac{Tf_{sol}}{Tf_{air}} \qquad \text{(Eq 1)}$$

where Tf_{sol} and Tf_{air} correspond to the time-to-failure obtained in solution and in air, respectively. Generally, a high value of r_{SCC} suggests the better SCC resistance of the alloy. In particular, the value of 1 indicates that the material exhibits no stress corrosion. Based on Eq 1, the r_{SCC} is calculated, and results are listed in Table 3. It reveals that the

T651 alloy (r_{SCC} = 0.8) possesses the largest SCC susceptibility among the three tempers, while T7351 and T7651 tempers can effectively improve the SCC resistance. Note that the SCC susceptibility of T7651 alloy (r_{SCC} = 0.91) is slightly larger than that of T7351 alloy (r_{SCC} = 0.95).

SEM observation at the edges of the SSRT samples failed in aqueous chloride solution is shown in Fig. 6. The fracture surface of T651 alloy exhibits severe SCC attack with intergranular fracture. However, the fractographs of T7351 and T7651 alloys reveal the absence of intergranular fracture. In the middle region of the fractograph (Fig. 6e, f), copious dimples are observed, showing a ductile fracture. In the region close to the fracture surface, the fracture shows cleavage like features as shown in Fig. 6(b) and (c). Comparing the overaged alloys, the T7351 alloy displays less cleavage facets but with more dimples. This fractograph observation implies that T7351 alloy has higher SCC resistance than that of T7651 alloy and is consistent with the r_{SCC} result.

The difference in SCC behavior can be correlated to the microstructure. For Al-Zn-Mg-Cu alloys, the dominant mechanism of SCC is proposed to be a chemical reaction caused by a combined action of anodic dissolution and hydrogen embrittlement (Ref 29, 30). The η (MgZn$_2$) precipitates on grain boundaries are more anodic than the aluminum matrix. As a result, these phases are preferentially attacked in chloride solution. Under the influence of the tensile stress applied on crack tip, the grain boundaries separate at a stress level much lower than the yield strength of this material. Accordingly, the continuous distribution of precipitates on grain boundaries will lead to a higher crack growth rate and facilitate serious SCC attack in T651 alloy. As evident from the SSRT results (Table 3) and fracture morphology (Fig. 6), overaging remarkably enhances SCC resistance. The mechanism can be explained as follows. Both T7351 and T7651 alloys in Fig. 1(c) and (f) exhibit discontinuously and coarse grain boundary precipitates. In this case, the anodic dissolution along grain boundaries is interrupted by the discontinuous precipitates. Besides, the coarse precipitates can reduce hydrogen content in grain boundaries because of the formation of hydrogen bubbles from the atomic hydrogen trapped by large grain boundary precipitates. Once the hydrogen concentration is reduced below a critical value, the hydrogen embrittlement process will be retarded (Ref 31).

The SCC process contains a crack initiation followed by the crack propagation. In the case of T651 alloy (in Fig. 6a), the dissolution of grain boundary precipitates provides initiation sites for corrosion crack. Once the crack propagates along the grain boundaries, the alloy shows low SCC resistance. On the other hand, a transition from brittle fracture mode to ductile fracture mode occurs when the alloy is subjected to overaging treatments (Fig. 6b, c). This result indicates that except for the anodic dissolution of η phase, the resistance to the crack propagation is another important factor to control the SCC susceptibility of overaged alloys. Furthermore, the fracture surfaces of two overaged alloys confirm that T7351 alloy exhibits a high proportion of transgranular fracture as well as a higher resistance to SCC. A reasonable explanation for such difference is that T7351 alloy increases the homogeneity of deformation and therefore improves the cracking resistance, as discussed in section 3.3. This is in agreement with the conclusion of Gruhl (Ref 32) who pointed out that the homogeneous slip can inhibit hydrogen embrittlement by effectively reducing hydrogen transport to the grain boundaries.

4. Conclusions

The tensile properties, FCP behavior and stress SCC of an Al-Zn-Mg-Cu alloy subjected to two overaging treatments are systematically investigated. For comparison, the peak-aged alloy is also tested. TEM micrograph shows that η' precipitate is the predominant strengthening phase in both T7351 and T7651 alloys. However, the main precipitates are larger in size with a low density in T7351 alloy as compared to that of T7651 alloy. This microstructure enables the relatively lower strength but higher electrical conductivity of T7351 alloy. Fatigue crack growth behavior reveals that the FCP resistance of T7351 alloy is superior to that of T7651 alloy. The main reason for this enhanced FCP resistance can be attributed to the coarser precipitates that reduce the strain localization by promoting homogeneous slip and thus result in a delay of crack nucleation. Both the SSRT test and fractograph observation suggest that overaged treatment can substantially improve the SCC resistance. The T7351 alloy has higher SCC resistance than T7651 alloy. The enhanced SCC resistance is found to depend on the grain boundary precipitate and the crack propagation resistance of the alloy.

References

1. R. Yang, Z. Liu, P. Ying, J. Li, L. Lin, and S. Zeng, Multistage-Aging Process Effect on Formation of GP Zones and Mechanical Properties in Al-Zn-Mg-Cu alloy, *Trans. Nonferrous Metals Soc*, 2016, **26**, p 1183–1190

2. L.K. Berg, J. Gjønnes, V. Hansen, X.Z. Li, M. Knustson-Wedel, G. Wateerloo, D. Schryvers, and L.R. Wallenberg, GP-Zones in Al-Zn-Mg Alloys and Their Role in Artificial Aging, *Acta Mater.*, 2001, **49**, p 3443–3451

3. J. Buha, R.N. Lumley, and A.G. Crosky, Secondary Ageing in an Aluminium Alloy 7050, *Mater. Sci. Eng. A*, 2008, **492**, p 1–10

4. K. Ma, H. Wen, T. Hu, T.D. Topping, D. Isheim, D.N. Seidman, E.J. Lavernia, and J.M. Schoenung, Mechanical Behavior and Strengthening Mechanisms in Ultrafine Grain Precipitation-Strengthened Aluminum Alloy, *Acta Mater.*, 2014, **62**, p 141–155

5. H.B. Larsen, G. Thorkildsen, S. Natland, and P. Pattison, Average Crystal Structure(s) of the Embedded Meta Stable η'-Phase in the Al-Mg-Zn system, *Philos. Mag.*, 2014, **94**, p 1719–1743

6. J. Chen, L. Zhen, S. Yang, W. Shao, and S. Dai, Investigation of Precipitation Behavior and Related Hardening in AA 7055 Aluminum Alloy, *Mater. Sci. Eng. A*, 2009, **500**, p 34–42

7. L. Lin, Z. Liu, S. Bai, P. Ying, and X. Wang, Effects of Germanium on Quench Sensitivity in Al-Zn-Mg-Zr Alloy, *Mater. Des.*, 2015, **86**, p 679–685

8. L. Lin, Z. Liu, Y. Li, X. Han, and X. Chen, Effects of Severe Cold Rolling on Exfoliation Corrosion Behavior of Al-Zn-Mg-Cu-Cr Alloy, *J. Mater. Eng. Perform.*, 2012, **21**, p 1070–1075

9. M.A. Krishnan and V.S. Raja, Development of High Strength AA 7010 Aluminum Alloy Resistant to Environmentally Assisted Cracking, *Corros. Sci.*, 2016, **109**, p 94–100

10. M. Talianker and B. Cina, Retrogression and Reaging and the Role of Dislocations in the Stress Corrosion of 7000-Type Aluminum Alloys, *Metall. Mater. Trans. A*, 1989, **20**, p 2087–2092

11. R. Goswami, S. Lynch, N.J.H. Holroyd, S.P. Knight, and R.L. Holtz, Evolution of Grain Boundary Precipitates in Al 7075 Upon Aging and Correlation with Stress Corrosion Cracking Behavior, *Metall. Mater. Trans. A*, 2013, **44**, p 1268–1278

12. S.P. Knight, K. Pohl, N.J.H. Holroyd, N. Birbilis, P.A. Rometsch, B.C. Muddle, R. Goswami, and S.P. Lynch, Some Effects of Alloy Composition on Stress Corrosion Cracking in Al-Zn-Mg-Cu Alloys, *Corros. Sci.*, 2015, **98**, p 50–62

13. L. Lin, Z. Liu, P. Ying, and M. Liu, Improved Stress Corrosion Cracking Resistance and Strength of a Two-Step Aged Al-Zn-Mg-Cu Alloy Using Taguchi Method, *J. Mater. Eng. Perform.*, 2015, **24**, p 4870–4877

14. P.K. Rout, M.M. Ghosh, and K.S. Ghosh, Influence of Aging Treatments on Alterations of Microstructural Features and Stress Corrosion Cracking Behavior of an Al-Zn-Mg Alloy, *J. Mater. Eng. Perform.*, 2015, **24**, p 2792–2805

15. N.J.H. Holroyd and G.M. Scamans, Stress Corrosion Cracking in Al-Zn-Mg-Cu Aluminum Alloys in Saline Environments, *Metall. Mater. Trans. A*, 2013, **44**, p 1230–1253

16. F. Wang, B. Xiong, Y. Zhang, B. Zhu, H. Liu, and X. He, Effect of Heat Treatment on the Microstructure and Mechanical Properties of the Spray-Deposited Al-10.8 Zn-2.8 Mg-1.9 Cu alloy, *Mater. Sci. Eng. A*, 2008, **486**, p 648–652

17. M. Song, Modeling the Hardness and Yield Strength Evolutions of Aluminum Alloy with Rod/Needle-Shaped Precipitates, *Mater. Sci. Eng. A*, 2007, **443**, p 172–177

18. P.K. Rout, M.M. Ghosh, and K.S. Ghosh, Microstructural, Mechanical and Electrochemical Behaviour of a 7017 Al-Zn-Mg Alloy of Different Tempers, *Mater. Charact.*, 2015, **104**, p 49–60

19. V.K. Gupta and S.R. Agnew, Fatigue Crack Surface Crystallography Near Crack Initiating Particle Clusters in Precipitation Hardened Legacy and Modern Al-Zn-Mg-Cu Alloys, *Int. J. Fatigue*, 2011, **33**, p 1159–1174

20. P.M.G.P. Moreira, P.F.P. de Matos, and P.M.S.T. de Castro, Fatigue Striation Spacing and Equivalent Initial Flaw Size in Al 2024-T3 Riveted Specimens, *Theor. Appl. Fract. Mech.*, 2005, **43**, p 89–99

21. S. Bai, Z. Liu, Y. Gu, X. Zhou, and S. Zeng, Microstructures and Fatigue Fracture Behavior of an Al-Cu-Mg-Ag Alloy with a Low Cu/Mg Ratio, *Mater. Sci. Eng. A*, 2011, **530**, p 473–480

22. F. Li, Z. Liu, W. Wu, P. Xia, P. Ying, Q. Zhao, J. Li, S. Bai, and C. Ye, On the Role of Texture in Governing Fatigue Crack Propagation Behavior of 2524 Aluminum Alloy, *Mater. Sci. Eng. A*, 2016, **669**, p 367–378

23. Z. Liu, F. Li, P. Xia, S. Bai, Y. Gu, D. Yu, and S. Zeng, Mechanisms for Goss-Grains Induced Crack Deflection and Enhanced Fatigue Crack Propagation Resistance in Fatigue Stage II, of an AA2524 Alloy, *Mater. Sci. Eng. A*, 2015, **625**, p 271–277

24. D. Yin, H. Liu, Y. Chen, D. Yi, B. Wang, B. Wang, F. Shen, S. Fu, C. Tang, and S. Pan, Effect of Grain Size on Fatigue-Crack Growth in 2524 Aluminium Alloy, *Int. J. Fatigue*, 2016, **84**, p 9–16

25. Z.Q. Zheng, B. Cai, T. Zhai, and S.C. Li, The Behavior of Fatigue Crack Initiation and Propagation in AA2524-T34 Alloy, *Mater. Sci. Eng. A*, 2011, **528**, p 2017–2022

26. Y.L. Wang, Q.L. Pan, L.L. Wei, B. Li, and Y. Wang, Effect of Retrogression and Reaging Treatment on the Microstructure and Fatigue Crack Growth Behavior of 7050 Aluminum Alloy Thick Plate, *Mater. Des.*, 2014, **55**, p 857–863

27. L. Lin, Z. Liu, W. Liu, Y. Zhou, and T. Huang, Effects of Ag Addition on Precipitation and Fatigue Crack Propagation Behavior of a Medium-Strength Al-Zn-Mg Alloy, *J. Mater. Sci. Technol.*, 2018, **34**, p 534–540

28. T.S. Srivatsan, S. Anand, S. Sriram, and V.K. Vasudevan, The High-Cycle Fatigue and Fracture Behavior of Aluminum Alloy 7055, *Mater. Sci. Eng. A*, 2000, **281**, p 292–304

29. P.K. Rout, M.M. Ghosh, and K.S. Ghosh, Effect of Solution pH on Electrochemical and Stress Corrosion Cracking Behaviour of a 7150 Al-Zn-Mg-Cu alloy, *Mater. Sci. Eng. A*, 2014, **604**, p 156–165

30. X.D. Li, X.S. Wang, H.H. Ren, Y.L. Chen, and Z.T. Mu, Effect of Prior Corrosion State on the Fatigue Small Cracking Behaviour of 6151-T6 Aluminum Alloy, *Corros. Sci.*, 2012, **55**, p 26–33

31. A. Thakur, R. Raman, and S.N. Malhotra, Hydrogen Embrittlement Studies of Aged and Retrogressed-Reaged Al-Zn-Mg Alloys, *Mater. Chem. Phys.*, 2007, **101**, p 441–447

32. W. Gruhl, Stress Corrosion Cracking of High Strength Aluminum Alloys, *Chem. Inf.*, 1985, **16**, p 1–3